frontiers | Frontiers in Water

TYPE Original Research
PUBLISHED 19 February 2025
DOI 10.3389/frwa.2025.1499448

OPEN ACCESS

EDITED BY
Giuseppe Oliveto,
University of Basilicata, Italy

REVIEWED BY
Zhuobiao Ni,
South China Agricultural University, China
Matthijs Bonte,
MB-Water, Netherlands

*CORRESPONDENCE
Massimo Rolle
massimo.rolle@tu-darmstadt.de

RECEIVED 20 September 2024
ACCEPTED 31 January 2025
PUBLISHED 19 February 2025

CITATION
Wienkenjohann H, Bin Hudari MS, Mosthaf K, Vogt C, Nijenhuis I and Rolle M (2025) Combining microcosm biodegradation and reactive transport modeling to explore the feasibility of ATES-bioremediation approaches.
Front. Water 7:1499448.
doi: 10.3389/frwa.2025.1499448

Combining microcosm biodegradation and reactive transport modeling to explore the feasibility of ATES-bioremediation approaches

Henning Wienkenjohann[1], Mohammad Sufian Bin Hudari[2], Klaus Mosthaf[1], Carsten Vogt[2], Ivonne Nijenhuis[2] and Massimo Rolle[1,3]*

[1]Department of Environmental and Resource Engineering, Technical University of Denmark, Kongens Lyngby, Denmark, [2]Department of Isotope Biogeochemistry, Helmholtz Centre for Environmental Research - UFZ, Leipzig, Germany, [3]Institute of Applied Geosciences, Department of Materials and Geosciences, Technical University of Darmstadt, Darmstadt, Germany

This study presents a process-based model analysis of non-isothermal biodegradation of chlorinated ethenes in batch microcosm setups and field-scale remediation, combining Aquifer Thermal Energy Storage with *in situ* bioremediation (ATES-ISB). The features of the proposed modeling framework include: (i) kinetic multi-phase mass transfer and temperature-dependent biodegradation in batch systems, and (ii) multi-dimensional non-isothermal fluid flow, heat transport, and contaminant transport in a physically and chemically heterogeneous aquifer combined with temperature-dependent microbial kinetics. The model was used to analyze an experimental microcosm dataset of temperature-dependent reductive dehalogenation of chlorinated ethenes, from which maximum specific degradation rates were derived. A scenario modeling investigation is presented, considering an ATES-ISB intervention in an aquifer contaminated with trichloroethene, where heated groundwater is injected and lactate is delivered to stimulate *in situ* microbial activity and contaminant transformation. Four scenario parameters were varied to identify the optimal conditions for efficient bioremediation. High lactate concentrations and temperatures at 20°C and 30°C led to more complete transformation of chlorinated ethenes in the considered heterogeneous aquifer system. Furthermore, the pumping rate and the natural groundwater flow velocity were found to control the delivery of heated water and solutes, including lactate, in the aquifer. The outcomes of the scenario simulations performed in this study are useful for designing non-isothermal bioremediation interventions in groundwater systems polluted with organic contaminants.

KEYWORDS

microcosms, aquifer thermal energy storage, bioremediation, chlorinated ethenes, reactive transport modeling, scenario simulations

1 Introduction

Organic compounds, such as trichloroethene (TCE) and its transformation products cis-1,2-dichloroethene (cis-DCE) and vinyl chloride (VC), are widespread contaminants in groundwater systems due to their intense use in industrial activities (McCarty, 2010). A large number of groundwater contaminated sites occur in industrial and urban areas and pose a risk

to humans and environmental systems (Rosenberg et al., 2023). Concurrently, heating and cooling demand is highest in urban and industrial areas (Epting et al., 2013). To balance out demand and supply, industrial waste heat or waste heat derived from the cooling of buildings can be stored in porous aquifer systems (Ueckert and Baumann, 2019). Aquifer Thermal Energy Storage (ATES) makes use of the subsurface to store heat energy. ATES setups are open-loop systems, in which cold groundwater is abstracted, heated, and reinjected into the porous aquifer. The flow direction is reversed in winter times, so that warm groundwater can be extracted and used for residential heating (Kumar et al., 2024). Pilot-scale experiments of ATES systems have shown energy recovery rates of around 66–89% (Molz et al., 1981; Heldt et al., 2024).

Remediation of chlorinated ethenes in heterogeneous groundwater systems is challenging due to the physico-chemical properties of these compounds, such as their high mobility and limited degradability (Pankow and Cherry, 1996). In the last decades, *in situ* bioremediation (ISB) has become one of the primary techniques to clean up sites contaminated with chlorinated ethenes since it results in contaminant transformation and effective mass removal (Major et al., 2002; Hood et al., 2008; Scheutz et al., 2008). Under favorable biogeochemical conditions, i.e., in anoxic aquifers, chlorinated ethenes can be dehalogenated by specialized indigenous bacteria, i.e., organohalide-respiring bacteria (OHRB) (Nijenhuis et al., 2007, 2013; Ottosen et al., 2021). Biostimulation of polluted aquifer systems can overcome the lack of available electron donor, and, concurrently, improve redox conditions in the groundwater system (Yamazaki et al., 2020). Bioaugmentation might be necessary in cases where no OHRB are present in the subsurface (Stroo et al., 2010). The temperature in the groundwater system is an important parameter determining the growth of indigenous and bioaugmented bacteria consortia in polluted aquifers (Friis et al., 2007a; Zeman et al., 2014). Former studies reported optimal microbial growth rates of OHRB, which are capable of biotransforming chlorinated ethenes, at a temperature range of 22–38°C (Friis et al., 2007b; Fletcher et al., 2011; Marcet et al., 2018). This is about the same temperature range at which low-temperature ATES systems are typically operated. Therefore, several studies have investigated the potential synergies of underground thermal energy storage systems with *in situ* bioremediation. This includes experimental laboratory studies (Ni et al., 2015, 2018), pilot-scale studies (Němeček et al., 2018; Wienkenjohann et al., 2024), and field-scale simulations (Zuurbier et al., 2013; Popp et al., 2015; Beyer et al., 2016; Meng et al., 2021; Roohidehkordi and Krol, 2021).

One important challenge during bioremediation interventions is to determine the rate of the naturally occurring biodegradation caused by indigenous bacteria in the contaminated aquifer system and to evaluate the effect of biostimulation. In this regards, microcosm studies have shown to be a versatile and useful tool (Allen-King et al., 1995; Malaguerra et al., 2011; Scheutz et al., 2014; Yu et al., 2018). Microcosm experiments can be used to assess the natural degradation potential at a contaminated site (Hunkeler et al., 1999), to demonstrate the effect of biostimulation during reductive dehalogenation (Yu et al., 2018), to understand the effect of bioaugmentation (Friis et al., 2007c), and to understand the competition within different microbial communities (Murray et al., 2020). However, only a few studies have used microcosms to investigate the effect of temperature on the biotransformation rate of chlorinated ethenes (Friis et al., 2005; Bin Hudari et al., 2025).

The combination of ATES and ISB induces a complex interplay between physical and biogeochemical processes (Wienkenjohann et al., 2024). These processes are temperature-dependent and govern the mobility and fate of pollutants, such as chlorinated ethenes, in subsurface porous media. Fluid flow is affected by heat transport, which also impacts solute transport, mixing and biogeochemical reactions in aquifer systems. To account for these challenging multi-physics phenomena, numerical simulators are needed, to effectively incorporate the coupled, physical and biogeochemical processes that occur during ATES-ISB. In addition, such numerical models allow the simulation of field-scale remediation interventions considering different scenarios (Popp et al., 2015; Beyer et al., 2016). Therefore, scenario simulations are a useful approach to test various flow, heat transfer and solute transport conditions and different operational procedures, which, ultimately, could lead to an optimal set of conditions and parameters for ATES-ISB interventions.

In this study, we present a batch multi-phase kinetic mass-transfer model and a field-scale model with scenario simulations to describe non-isothermal reactive transport and biodegradation of chlorinated ethenes. Temperature-dependent maximum specific degradation rates are derived from the model-based analysis of microcosm setups and used as input for reactive transport simulations of a modeled ATES-ISB intervention in a physically and chemically heterogeneous aquifer, which is contaminated with chlorinated ethenes. Field-scale scenario modeling in the considered groundwater system was performed to assess the biodegradation potential considering four operational constraints: (i) the natural groundwater flow velocity, (ii) the pumping rate of the injection/abstraction system, (iii) the injection temperature, and (iv) the injected concentration of lactate as substrate to stimulate microbial growth and biological reductive dehalogenation. Finally, we also discuss the optimal parameter set for field-scale ATES-ISB at sites contaminated with chlorinated ethenes.

2 Laboratory and field-scale setups

A conceptual, multi-scale representation of the microcosms and a field-scale system is shown in Figure 1. In the multi-phase microcosms, mass transfer of contaminants can occur between the sediment, water, and gas phase and microbial reductive dechlorination is carried out by indigenous dehalogenators (i.e., *Dehalococcoides* spp., *Dhc*) (Figure 1a). The reactive field-scale setup includes active pumping with injection of warm groundwater, its recirculation, and biostimulation of the system with lactate (Figures 1b,c). Four key parameters (one site parameter and three operational parameters) are varied to assess the overall biotransformation potential in different modeling scenarios (Figure 1d).

2.1 Description of microcosm dataset

The dataset used in this study was obtained from microcosm experiments performed in a three-phase system comprising aquifer sediments, an aqueous phase, and a gas phase. Bin Hudari et al. (2025) provide a detailed description of the experimental procedures and materials. Briefly, 20 g of aquifer sediments polluted with TCE from a contaminated site in Ferrara, Northern Italy, were prepared in 125 mL

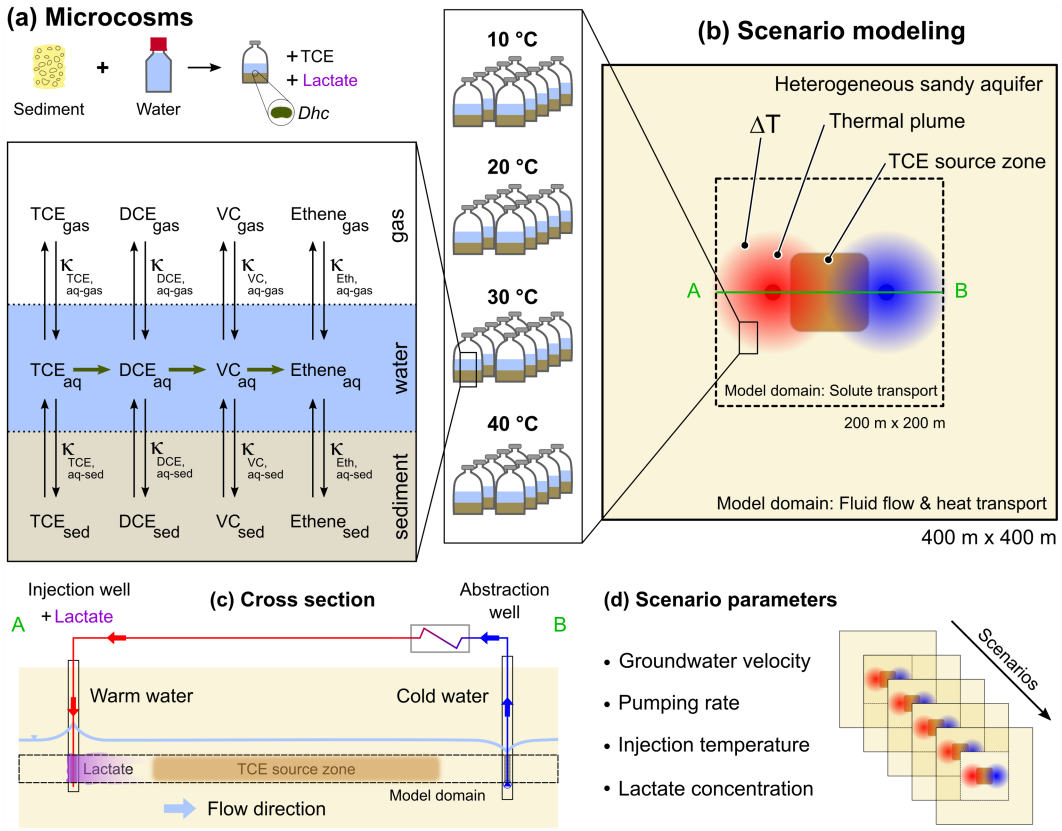

FIGURE 1
Schematic representation of the multi-scale approach incorporating microcosm biodegradation and field-scale reactive transport modeling. Incubation of biostimulated microcosms at four different temperatures and batch multi-phase modeling **(a)**. Field-scale scenario modeling approach combining Aquifer Thermal Energy Storage with *in situ* bioremediation (ATES-ISB) in a two-dimensional aquifer system **(b,c)**. Scenario parameters considered in field-scale simulations **(d)**.

serum bottles each filled with 50 mL of aqueous mineral salts medium in an anoxic chamber. The bottles were fitted with Teflon-lined caps and crimped tightly. The microcosms were amended with 3 mM of lactate as substrate at day 0 and were incubated for 105 days at 10°C, 20°C, 30°C, and 40°C. The systems held at 20°C and 30°C were spiked with 100 µM of TCE at day 3, 35, 56, and 70 and chlorinated ethene concentrations were measured in the headspace to investigate the effect of temperature on the biodegradation potential of the indigenous bacterial consortium (Figure 1a).

2.2 Geometry and design of field-scale simulations

In order to explore the feasibility of ATES-bioremediation approaches, a field-scale reactive transport model was employed (Figures 1b,c. The proposed model used the biodegradation kinetics determined in the microcosm system. We assumed an aquifer with a thickness of 6 m and a width and length of 400 meters. A contaminant source was placed in the center of the aquifer. The source consisted of TCE, present as aqueous phase and free, non-aqueous phase liquid (NAPL) (Supplementary Figure S2). Two wells were located in the center of the aquifer to represent a recirculation system, operated as in ATES-ISB systems (Wienkenjohann et al., 2024). The eastern well was used for the abstraction of groundwater, whereas the western well was used to inject the heated groundwater back into the subsurface (Figure 1b). The model included indigenous *Dhc* bacteria, capable of transforming TCE to the non-toxic end product ethene. These OHRB were present, bound to the sediments, in the entire solution domain. Dissolved organic carbon and lactate were considered as substrate providing carbon sources and electron donors. Lactate was injected via the injection well into the system, whereas DOC was present at a pristine background concentration from the start of the simulation. The chemical species were advectively transported by the natural groundwater flow and active pumping. The physics of the fluid flow, solute transport, and biogeochemical reactions were coupled. The temperature dependence and non-isothermal properties of these processes were considered to accurately describe transport and biotransformation of the organic contaminants in the contaminated aquifer.

2.3 Modeling approach

2.3.1 Modeling of batch microcosms

2.3.1.1 Multi-phase kinetic mass transfer

The vertical, black arrows in Figure 1 represent the mass transfer of the chlorinated ethenes between the distinct phases (sediment, water,

and gas). In the model, reductive dehalogenation by *Dhc* is considered only for chlorinated ethenes dissolved in the aqueous phase. The change in concentration of each relevant species in each phase is described by a set of ordinary differential equations (Equations 1–3) (Aeppli et al., 2009; Jin et al., 2013; Murray et al., 2019):

$$\frac{dc_{aq,i}}{dt} = \frac{-\left(\frac{dn_i}{dt}\right)_{aq-gas}}{V_{aq}} + \frac{-\left(\frac{dn_i}{dt}\right)_{aq-sed}}{V_{aq}} - r_{deg} \quad (1)$$

$$\frac{dc_{sed,i}}{dt} = \frac{\left(\frac{dn_i}{dt}\right)_{gas-sed}}{V_{sed}} + \frac{\left(\frac{dn_i}{dt}\right)_{aq-sed}}{V_{sed}} \quad (2)$$

$$\frac{dc_{gas,i}}{dt} = \frac{-\left(\frac{dn_i}{dt}\right)_{gas-sed}}{V_{gas}} + \frac{\left(\frac{dn_i}{dt}\right)_{aq-gas}}{V_{gas}} \quad (3)$$

where $dc_{x,i} / dt$ [mol L^{-1} s^{-1}] is the change in concentration for the species i in phase x, V_x [L] is the volume of phase x, dn_i / dt [mol s^{-1}] represents the total, species-specific change in moles between the phases, and r_{deg} is the biodegradation rate. The gas and sediment phases do not share an interface, therefore $(dn_i / dt)_{gas-sed}$ is equal to zero. The initial concentration of TCE is highest in the aqueous phase. Thus, movement from the aqueous phase is defined as positive. The transfer of mass across the two relevant phase interfaces $(dn_i / dt)_{aq-gas}$ and $(dn_i / dt)_{aq-sed}$, can be described by Equations 4, 5 (Aeppli et al., 2009; Murray et al., 2019):

$$\left(\frac{dn_i}{dt}\right)_{aq-gas} = \left(\frac{\kappa_{aq-gas,i} A_{aq-gas}}{V_{aq}}\right) V_{gas} \left(c^{eq}_{gas,i} - c_{gas,i}\right) \quad (4)$$

$$\left(\frac{dn_i}{dt}\right)_{aq-sed} = \left(\frac{\kappa_{aq-sed,i} A_{aq-sed}}{V_{aq}}\right) V_{sed} \left(c^{eq}_{sed,i} - c_{sed,i}\right) \quad (5)$$

where $c_{x,i}$ [mol m^{-3}] and $c^{eq}_{x,i}$ [mol m^{-3}] are the concentration and equilibrium concentration of species i in the x-th phase, respectively, $\kappa_{aq-gas,i}$ [cm s^{-1}] and $\kappa_{aq-sed,i}$ [cm s^{-1}] are the species-specific mass transfer coefficients, while A_{x-x} [cm^2] is the cross-sectional area of the respective phase interface. More information on the model parameters and temperature-dependent mass transfer processes, including volatilization and sorption, is provided in the Supplementary material.

2.3.1.2 Temperature-dependent biodegradation and microbial dynamics

The temperature-dependent biodegradation and the dynamics of indigenous microorganisms were simulated as such that TCE was sequentially biotransformed to cis-DCE, VC, and ethene under anoxic conditions with dissolved organic carbon and lactate as electron donors' source. Organohalide-respiring bacteria were assumed as a *Dehalococcoides* containing bacterial consortium, which was attached to the sediment, and is capable of carrying out the complete transformation sequence from TCE to ethene.

For both the modeling of the microcosms and the field-scale scenario simulations, double-Monod kinetics including competitive inhibition of dissolved chlorinated ethenes were used to implement temperature-dependent biotransformation reactions, occurring in the aqueous phase (Yu and Semprini, 2004; Murray et al., 2019):

$$r_{deg} = \frac{\partial c_{EA_i}}{\partial t} = -\kappa_{max,EA_i,X_{Dhc}}(T)\left(\frac{c_{ED_n}}{c_{ED_n} + K_{s,ED_n}}\right)\left(\frac{c_{EA_i}}{c_{EA_i} + K_{s,EA_i}\left(1 + \sum_{j=1}^{n}\frac{c_{EA_j}}{K_{inh_j}}\right)}\right) X_{Dhc} \quad (6)$$

where c_{ED_n} is the molar concentration of the n-th electron donor (ED), $\kappa_{max,EA_i,X_k}(T)$ [s^{-1}] represents the maximum specific degradation rate at temperature T of the i-th electron acceptor (EA) (i.e., the chlorinated ethenes), X_{Dhc} is the molar concentration of the indigenous *Dhc* bacteria, K_{s,ED_n} [mol m^{-3}] represents the half-saturation constant of the n-th ED, and K_{s,EA_i} [mol m^{-3}] is the half-saturation constant of the i-th EA. The inhibition constant of K_{inh_j} [mol m^{-3}] of the j-th EA is considering all the other electron acceptors, except the i–th EA.

Growth and decay of biomass are described as:

$$\frac{\partial X_{Dhc}}{\partial t} = -\mathrm{Y}\frac{\partial c_{EA_i}}{\partial t} - b_{Dhc} X_{Dhc} \quad (7)$$

in which the bacterial yield Y was implemented with a value of 0.02 [mol_X mol_{EA}^{-1}] (Malaguerra et al., 2011), and b_{Dhc} [s^{-1}] is the biomass decay coefficient (Cupples et al., 2004).

2.3.2 Field-scale simulations

2.3.2.1 Non-isothermal flow and heat transport

Field-scale non-isothermal fluid flow in a saturated porous aquifer can be described by the following governing equation (Equation 8) (Bear and Bachmat, 1990):

$$\frac{\partial\left(n\rho_l(T)\right)}{\partial t} = \nabla\cdot\left(\rho_l(T)\frac{\boldsymbol{k}}{\eta(T)}\left(\nabla p - \rho_l(T)\boldsymbol{g}\right)\right) + Q_F \quad (8)$$

in which n is the porosity [−], ρ_l is the water density [kg m^{-3}], t is time [s], $\boldsymbol{k}$ stands for the intrinsic permeability tensor [m^2], η is the dynamic viscosity of water [kg m^{-1} s^{-1}], p is the water pressure [kg m^{-1} s^{-2}], $\boldsymbol{g}$ is the vector of gravitational acceleration [m s^{-2}], and Q_F is a source/sink term [kg m^{-3} s^{-1}].

The temperature dependence of water density, water viscosity, specific isobaric heat capacity of water, and the thermal conductivity of water were implemented using the IF97 formulation (Wagner et al., 2000; IAPWS, 2007), resulting in temperature-induced changes in the

hydraulic conductivity tensor $\boldsymbol{K}$, whereas the intrinsic permeability $\boldsymbol{k}$ is a specific property of the solid matrix of the porous medium.

The heat convection-conduction (Equation 9) (e.g. Bear and Bachmat, 1990; Sprocati et al., 2023) was used to describe non-isothermal heat transport in the field-scale groundwater system:

$$\frac{\partial\left(\left(\rho c_p\right)_{eff} T\right)}{\partial t} = -\nabla\cdot\left(n\rho c_p \boldsymbol{v} T\right) + \nabla\cdot\left(\boldsymbol{D}_H \nabla T\right) + Q_H \tag{9}$$

where c_p [J kg^{-1} K] is the specific heat capacity of the porous medium, $\boldsymbol{v}$ is the seepage velocity vector, $\boldsymbol{D}_H$ is the heat dispersion tensor, and Q_H is a term for the source/sink of heat. The effective volumetric heat capacity $\left(\rho c_p\right)_{eff}$ of the porous medium (Equation 10), with the subscripts l and s indicating the liquid phase and the solid matrix, respectively, can be written as:

$$\left(\rho c_p\right)_{eff} = n\rho_l c_{p,l} + \left(1-n\right)\rho_s c_{p,s} \tag{10}$$

The tensor for the dispersion of heat in the porous media is shown in Equation 11:

$$\boldsymbol{D}_H = \boldsymbol{\lambda}_{cond,eff} + \boldsymbol{\lambda}_{disp,eff} \tag{11}$$

where the effective thermal conductivity tensor $\boldsymbol{\lambda}_{cond,eff}$ [W m^{-1} K^{-1}] (Equation 12) can be approximated from the porosity and the thermal conductivity of the fluid ($\boldsymbol{\lambda}_l$) and the solid phase ($\boldsymbol{\lambda}_s$) (Zimmerman, 1989):

$$\boldsymbol{\lambda}_{cond,eff} = n\lambda_l\delta_{ij} + \left(1-n\right)\lambda_s\delta_{ij} \tag{12}$$

in which $\delta_{ij}\left[-\right]$ is the Kronecker delta. The effective thermal dispersion tensor $\boldsymbol{\lambda}_{disp,eff}$ reads as (Equation 13):

$$\boldsymbol{\lambda}_{disp,eff} = n\rho_l c_{p,l}\left(\gamma_T\left|\boldsymbol{v}\right|\delta_{ij} + \left(\gamma_L-\gamma_T\right)\frac{v_i v_j}{\left|\boldsymbol{v}\right|}\right) \tag{13}$$

where γ_L and γ_T [m] are, respectively, the longitudinal and transverse thermal dispersivities, and v_i and v_j [m s^{-1}] are the components of the seepage velocity in i and j directions, respectively.

2.3.2.2 Reactive transport

Reactive solute transport at field scale is described by the advection-dispersion-reaction equation (Bear and Bachmat, 1990) as shown in Equation 14:

$$R_i\left(T\right)\frac{\partial\left(nc_i\right)}{\partial t} = -\nabla\cdot\left(n\boldsymbol{v}c_i\right) + \nabla\cdot\left(n\boldsymbol{D}_i\nabla c_i\right) - nr_{deg} \tag{14}$$

where R_i is the retardation factor of the transported species i, c_i is the molar concentration of the species i, and $\boldsymbol{D}_i$ is the local hydrodynamic dispersion tensor with the components D_i^L and D_i^T in longitudinal and transverse direction, respectively. The local longitudinal dispersion coefficient (Equation 15) (Guedes de Carvalho and Delgado, 2005; Muniruzzaman and Rolle, 2017) and the local transverse dispersion coefficient (Equation 16) (Chiogna et al., 2010; Rolle et al., 2012) were implemented as follows:

$$D_i^L = D_i^P + \frac{1}{2}\left|\boldsymbol{v}\right|d \tag{15}$$

$$D_i^T = D_i^P + D_i^{aq}\left(\frac{Pe_i^2}{Pe_i + 2 + 4\delta^2}\right)^{\beta} \tag{16}$$

in which d [m] is the spatially-varying grain size diameter of the aquifer material, $D_i^P \approx D_i^{aq} n$ [m^2 s^{-1}] is the pore diffusion coefficient, D_i^{aq} is the aqueous diffusion coefficient [m^2 s^{-1}], $Pe = \left|\boldsymbol{v}\right|d \,/\, D_i^{aq}$ is the dimensionless grain Péclet number, δ [−] is the ratio between the length of a pore channel and its hydraulic radius, and β [−] is an empirical parameter accounting for the effects of incomplete mixing in the pores. We consider values of δ and β (5.37 and 0.5, respectively) as reported in Ye et al. (2015).

In this paper, hydraulic aquifer characteristics of the well-studied Borden aquifer (Ontario, Canada) were used (Sudicky, 1986) (Supplementary Table S1) to create a heterogeneous hydraulic conductivity field (Wienkenjohann et al., 2023) (more information is provided in the Supplementary material). The heterogeneity of the hydrogeological subsurface impacts field-scale contaminant transport. In order to accurately simulate the transport of contaminants in the subsurface, a spatially variable description of the porosity, grain size, and fraction of organic carbon was implemented using the same procedure as described in detail in Wienkenjohann et al. (2024). Probability density functions of the spatial random fields are shown in Supplementary Figure S3.

The aqueous diffusion coefficients are compound-specific and different for the distinct chlorinated ethenes (Rolle et al., 2013; Jin et al., 2014). Their value and temperature dependence (Equation 17) was calculated according to Worch (1993):

$$D_i^{aq}\left(T\right) = 3.595\times10^{-14}\frac{T}{\eta M_i^{0.53}} \tag{17}$$

where M_i [g mol^{-1}] is the molecular mass of the i-th species. The increase of aqueous diffusion coefficients with increasing temperature for the chlorinated ethenes considered in this study is shown in Supplementary Figure S1B.

Temperature-dependent sorption of chlorinated ethenes to the sediment was implemented by linear equilibrium sorption (Equation 18). The resulting temperature-dependent retardation factor reads as:

$$R_i\left(T\right) = 1 + \frac{\rho_b}{n}K_i^d\left(T\right) \tag{18}$$

in which ρ_b is the bulk density of the sediment, and $K_i^d\left(T\right) = K_i^{OC}\left(T\right) f_{OC}$ is the sorption distribution coefficient, with K_i^{OC} (T) [L kg^{-1}] being the temperature-dependent species-specific

soil organic carbon-water partition coefficient as shown in Supplementary Figure S1D, and f_{OC} [−] the spatially varying fraction of organic carbon in the sediment (Supplementary Figure S3D).

The proposed field-scale model also accounts for temperature-dependent kinetic mass transfer between the free TCE phase (non-aqueous phase liquid (NAPL)), and the aqueous TCE phase. The NAPL phase dissolves and progressively releases TCE in the groundwater. The aqueous solubility is dependent on temperature and was implemented following an empirical model proposed by Koproch et al. (2019) (Supplementary Figure S1A). The linear driving force expression, with temperature-dependent aqueous solubility, can be used to describe inter-phase mass transfer (Equation 19) (Powers et al., 1994):

$$\frac{dc_i}{dt} = \omega_i \left(S_i(T) - c_i \right) \tag{19}$$

in which ω_i is the mass-transfer rate as reported in Illy et al. (2022), S_i is the temperature-dependent aqueous solubility (Supplementary Figure S1A), and c_i is the species-specific aqueous concentration. In this study, only TCE has been included as NAPL in the model.

The reactive term r_{deg} is expressed with a double-Monod kinetics (Equation 6) representing a mixing-controlled reaction between the electron donors and electron acceptors in the aquifer system (Rolle and Le Borgne, 2019; Valocchi et al., 2019). The dynamics of the indigenous reductive dehalogenators in the simulated aquifer system was described as in Equation 7, since it was assumed that the bacteria are attached to the solid matrix of the aquifer and, thus, do not undergo transport processes (Bauer et al., 2009; Griebler and Lueders, 2009).

2.3.2.3 Model implementation

The field-scale model domain is split into two solution domains. One large 400 m × 400 m domain for solving the fluid flow and heat transport, and a smaller 200 m × 200 m domain for solving the reactive solute transport (overview in Figure 1 and Supplementary Figure S2). Two wells were positioned 30 m apart in the center of the domain. The western well is the injection well and the eastern well is the abstraction well. No-flow boundary conditions were assigned to the top and bottom sides of the fluid flow domain. Fixed head boundary conditions were imposed at the western and eastern side of the domain. The injection and abstraction wells were implemented as point source/sink. Physical and chemical heterogeneity was implemented using spatial random fields based on aquifer characteristics as shown in Supplementary Table S1 and Supplementary Figure S3. We assumed an initial groundwater temperature of 10°C in the entire field-scale domain and set fixed temperature boundary conditions at the upstream and downstream sides of the domain, with no-flux boundary conditions at the top and bottom of the domain. A fixed temperature was assigned to the injection well, representing the re-injection of heated groundwater into the aquifer.

The reactive solute transport was solved in a smaller domain with finer spatial discretization and a very fine mesh around the wells, where high pressure and concentration gradients could be expected. We assigned no-flux boundary conditions to all sides of the solute transport domain, except to the eastern, downstream boundary and to the abstraction well, where outflow boundary conditions were set. Supplementary Figure S2 shows the initial distribution of TCE in the aqueous phase and in the free NAPL phase. All chemical species were recirculated in the ATES-ISB system by evaluating the species concentration at the abstraction well and re-injecting them at the injection well using a specified flux condition. Furthermore, we added a term for the addition of lactate at the injection well. The initial DOC concentration was set to 0.125 mM in the entire solute transport domain. Immobile *Dhc* bacteria were assumed present in the model domain from the beginning of the simulation. Detailed information on the model parameters is provided in the Supplementary material.

The entire model domain was spatially discretized by a mesh with 2.13×10^4 triangular elements. The mesh was refined where strong gradients were expected. The governing equations were solved with the finite-element simulation tool COMSOL Multiphysics® v6.1.

2.4 Scenario simulations

Scenario simulations were used to explore the feasibility of ATES-ISB interventions in an aquifer contaminated with chlorinated ethenes. We used four key scenario parameters: (i) the groundwater flow velocity under natural gradient conditions, (ii) the pumping rate of the injection/extraction ATES system, (iii) the temperature of the injected groundwater, and (iv) the concentration of the injected lactate. We used the same fields of permeability, porosity, grain diameter, and fraction of organic carbon in all scenarios to ensure comparable results. The scenarios were simulated for 360 days. Table 1 shows an overview of the sixteen scenarios that were explored in this work with the proposed numerical modeling approach described above.

Scenario S0 was used as a base case with optimal parameter values. The scenarios S1, S2, S3, and S4 explored the effect of different natural groundwater flow velocity, pumping rate, temperature of injected groundwater, and concentration of injected lactate on the overall biotransformation potential of the chlorinated ethenes in the contaminated aquifer. Scenarios S5 and S6 assessed in detail the effect of the natural groundwater velocity considering different combinations of operational parameter sets. The results of all scenarios were compared by means of total masses of each chlorinated ethene species integrated over the entire solution domain of the reactive solute transport problem (200 m × 200 m). The set of scenarios S1 to S4, including the base case S0, are shown in the main manuscript, whereas the results of the scenario sets S5 and S6 are reported in the Supplementary material.

3 Results and discussion

3.1 Simulation of temperature-dependent biodegradation in the microcosms

Chlorinated ethenes were biotransformed via sequential reductive dehalogenation in the microcosms. Figure 2 shows the experimental data from the microcosm studies (Bin Hudari et al., 2025), alongside with the outcome of the multi-phase biodegradation model for the four different temperatures

10.3389/frwa.2025.1499448

TABLE 1 Overview of ATES-ISB scenario simulations.

Scenario	Natural groundwater flow velocity [m/year]	Pumping rate [m³/h]	Temperature of injected groundwater [°C]	Concentration of injected lactate [mM]
S0	8	15	30	0.2
S1a	40	15	30	0.2
S1b	80	15	30	0.2
S2a	8	5	30	0.2
S2b	8	10	30	0.2
S3a	8	15	10	0.2
S3b	8	15	20	0.2
S3c	8	15	40	0.2
S4a	8	15	30	0.002
S4b	8	15	30	0.02
S5a	8	5	10	0.002
S5b	40	5	10	0.002
S5c	80	5	10	0.002
S6a	8	10	20	0.02
S6b	40	10	20	0.02
S6c	80	10	20	0.02

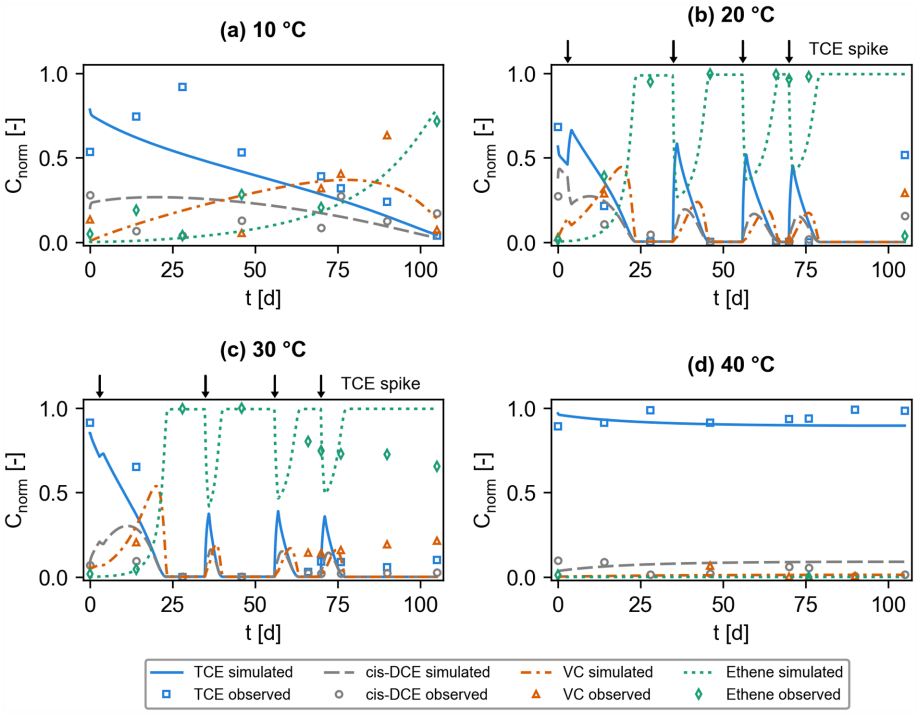

FIGURE 2
Observed markers; dataset obtained from Bin Hudari et al. (2025) and simulated (lines) normalized aqueous concentrations of chlorinated ethenes from batch microcosm setups at four different temperatures, **(a)** 10°C, **(b)** 20°C, **(c)** 30°C, and **(d)** 40°C. Additional TCE was spiked to microcosms operated at 20°C and 30°C after 3, 35, 56, and 70 days (arrows at top of panels **b,c**).

investigated in this work. Experimental data show incomplete reductive dehalogenation of TCE to ethene for microcosms at 10°C and 40°C, whereas complete dehalogenation was observed for the experiments at 20°C and 30°C. TCE concentrations decrease more rapidly at 20°C and 30°C compared to experiments conducted at 10°C, where transformation products, such as cis-DCE and VC accumulate. Experimental data at the highest temperature, i.e., 40°C, show stable values of TCE concentration,

indicating the lack of significant microbial reductive dehalogenation in these conditions. Considering the complexity of the setups with two fluid phases and a solid natural sediment, the kinetic interphase mass transfer between the phases, the temperature dependence, and the dynamic operational conditions (i.e., multiple spiking TCE spiking events for microcosms operated at 20°C and 30°C), the developed numerical model allows capturing most of the patterns and trends shown by the experimental observations. However, some trends were more difficult to capture, such as TCE concentrations observed in the microcosms held at 10°C. TCE is not entirely transformed to ethene in the first ~70 days of the microcosm experiments carried out at 10°C. This resulted in slow degradation in the first ~70 days and more complete degradation in the last period of the microcosms operated at 10°C. In addition, the gradual decrease of measured ethene in the microcosms held at 30°C might indicate further mass transfer or transformation of ethene. The accumulation of VC from day 65 onwards might indicate slower transformation rates of VC to ethene. The spiking events add new TCE mass to the systems operated at 20°C and 30°C, which is readily biotransformed under these optimal temperature conditions. The model indicates most complete reductive dehalogenation at 20°C and 30°C, where TCE is rapidly transformed to cis-DCE and VC, and these daughter compounds are further dehalogenated to ethene. The simulated slow dehalogenation kinetics at 10°C and the absence of biotransformation at 40°C are in line with the experimental observations collected from these respective microcosms.

In this study, the three maximum specific degradation rates of the chlorinated ethenes were adjusted to obtain a good fit between experimental data and simulation results. The fitted maximum specific degradation rates for each chlorinated ethene at each temperature (10°C, 20°C, 30°C, and 40°C), as derived from the simulation of the microcosms, are shown in Figure 3. The data show a clear temperature dependence with optimum temperatures for microbial dehalogenation at 29°C, 26°C, and 25°C for TCE, cis-DCE, and VC, respectively, as derived by fitting an empirical model (Rosso et al., 1995; Popp et al., 2015). The difference in optimal temperatures is in line with previous studies investigating the effect of temperature on microbial reductive dehalogenation of chlorinated ethenes (Friis et al., 2007b).

The temperature dependence of the maximum specific degradation rates, as shown in Figure 3, is a key input for the field-scale simulations of ATES-ISB scenarios and thus links the multi-phase microcosm studies to the field-scale modeling of non-isothermal remediation interventions.

3.2 Field-scale scenario simulations

Transient field-scale simulations, considering active pumping, heat transport, and reactive solute transport were conducted for a set of 16 scenarios with combinations of different parameters (Table 1).

3.2.1 Non-isothermal flow and heat transport

The groundwater flow field was changed by using natural groundwater velocities from 8 m/year to 80 m/year. Additionally, three different pumping rates were simulated in the ATES-ISB system. Figure 4 shows that the pumping induces a dipole flow field in the vicinity of the injection and extraction wells. The capture zone has the largest extent at low natural groundwater flow velocities (Figures 4a–c). These velocity variations, and irregular streamlines outside the capture zone, are caused by the physical heterogeneity in the simulated aquifer system. The zones of influence of the well-doublet system decrease in size at higher natural groundwater flow velocities. Nonetheless, even at 80 m/year and a pumping rate of 5 m^3/h, a dipole flow field is observed based on the simulated streamlines and velocity distribution. The size of the capture zone has important implications for the ATES-ISB application, since it impacts the subsurface contaminated zone that can be treated and where active delivery of amendments and reactants to stimulate microbial activities can occur.

The fluid flow is directly affecting the transport of heat in the simulated aquifer system. Figure 5 shows simulated surface maps of the temperature distribution at four times, at the beginning of the simulation (10 days), after 120 days, 240 days, and at the end of the simulation (360 days). The distribution of heat in the subsurface is evaluated at the three different natural groundwater flow velocities (i.e., 8, 40, and 80 m/year) considered in this study. Figures 5a–d indicate that the heat plume, which originates from the injection well, is not influenced much by the natural groundwater flow at low flow velocities. Contrarily, at higher natural groundwater flow velocities, the heat plume is significantly smaller and spreads in the flow

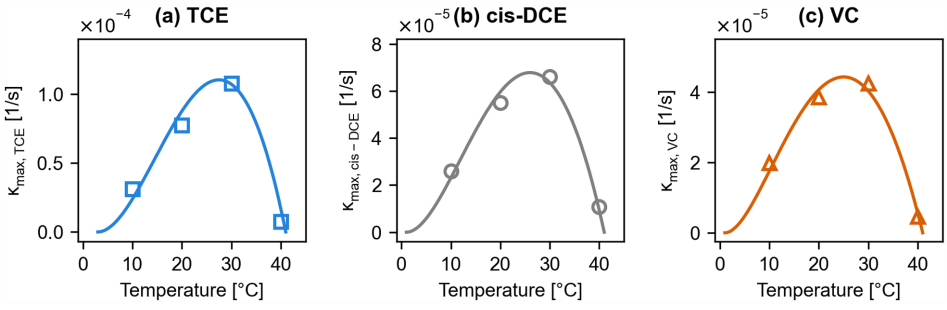

FIGURE 3
Temperature dependence of maximum specific dehalogenation rates of *Dhc* for trichloroethene (TCE) **(a)**, cis-1,2-dichloroethene (cis-DCE) **(b)**, and vinyl chloride (VC) **(c)**. Values derived from multi-phase modeling of experimental microcosms (Figure 2) (markers), and fitted with the empirical model by Rosso et al. (1995) (lines).

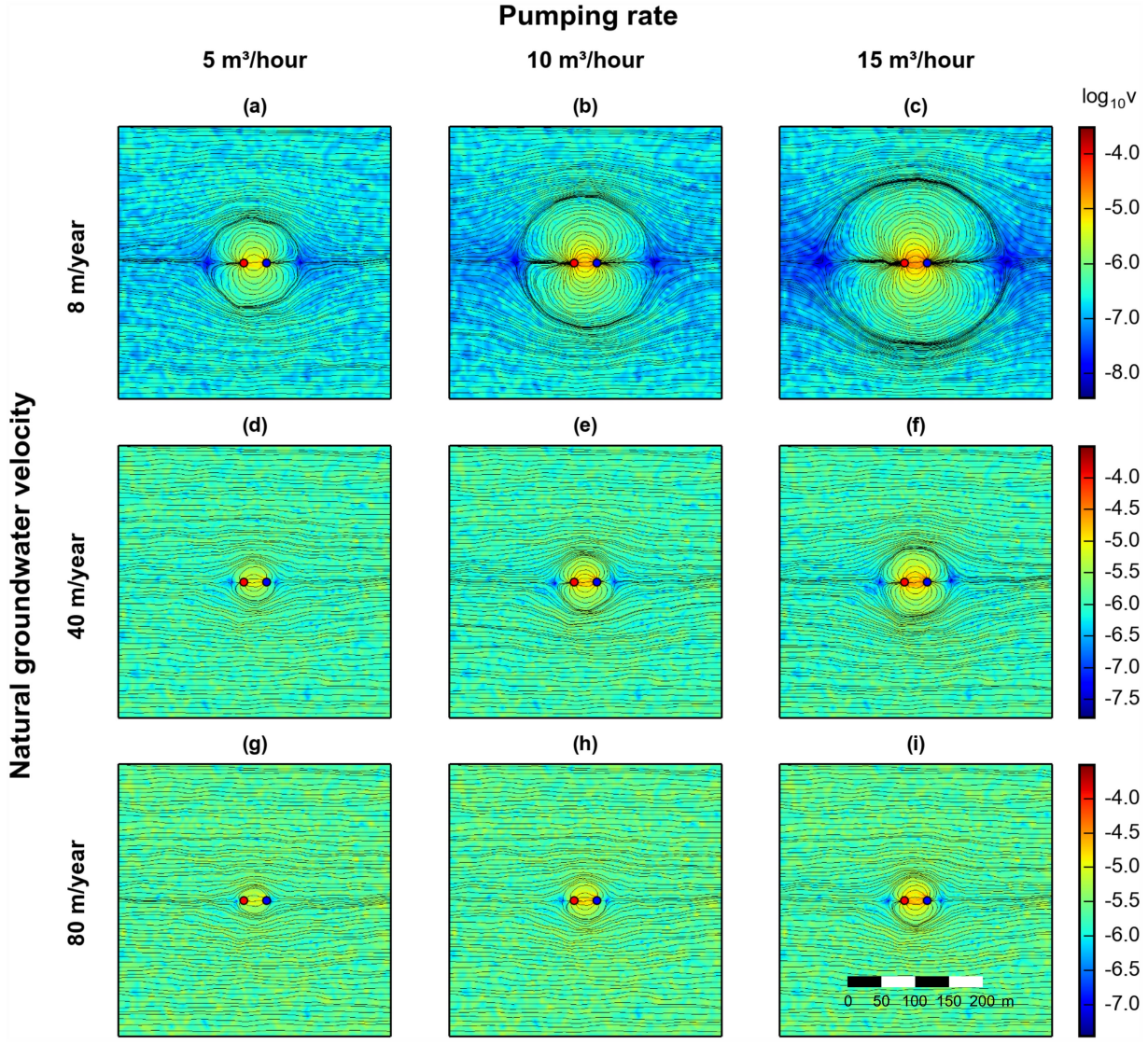

FIGURE 4
Simulated field-scale surface maps (isothermal conditions) of the groundwater flow velocity ($\log_{10}$ (**ν** [m s^{-1}])) with computed streamlines at three different natural groundwater flow velocities of **(a–c)** 8, **(d–f)** 40, and **(g–i)** 80 m/year (rows), and considering three different pumping rates, **(a,d,g)** 5, **(b,e,h)** 10, and **(c,f,i)** 15 m^3/h (columns). The natural groundwater flow direction is from left to right. Red and blue dots indicate the injection and extraction wells, respectively.

direction. Furthermore, the impact of groundwater flow on heat transport has important feedback also on the reactive contaminant transport, since the temperature distribution directly affects the transport parameters and the kinetics of biotransformation reactions.

3.2.2 Reactive transport model

The fluid and heat transport model laid the basis for the reactive transport model, which simulated the temperature-dependent biotransformation of chlorinated ethenes considering an ATES-ISB approach. Lactate, which serves as electron donor in this study, is delivered via active pumping into the contaminated aquifer. Figure 6 shows an example of the simulated spreading of lactate at the three natural groundwater velocities investigated in this study. Similarly to the transport of heat in the aquifer, the fluid flow significantly affects the distribution of lactate in the aquifer. The lactate spreads according to the induced dipole flow field at low flow velocities (Figures 5a–d), whereas a lactate plume is forming downgradient of the abstraction well at higher flow velocities (Figures 5i–l). Concurrently, the lactate plume is more spread at 8 m/year, with smooth concentration gradients in both longitudinal and transverse direction, compared to 40 m/year and especially 80 m/year flow velocity. In particular, at the highest natural groundwater flow velocity of 80 m/year, the concentration gradients are steep and sharply defined zones of lactate-rich and lactate-poor areas are present in the aquifer. Under these flow conditions, some lactate bypasses the extraction well and is transported advectively downstream towards the outflow boundary of the domain, though not reaching it at the end of the simulation time (360 days). The area of high lactate concentrations is smaller at high flow velocity, as evident from the surface maps at the last time step (Figures 6d,h,i).

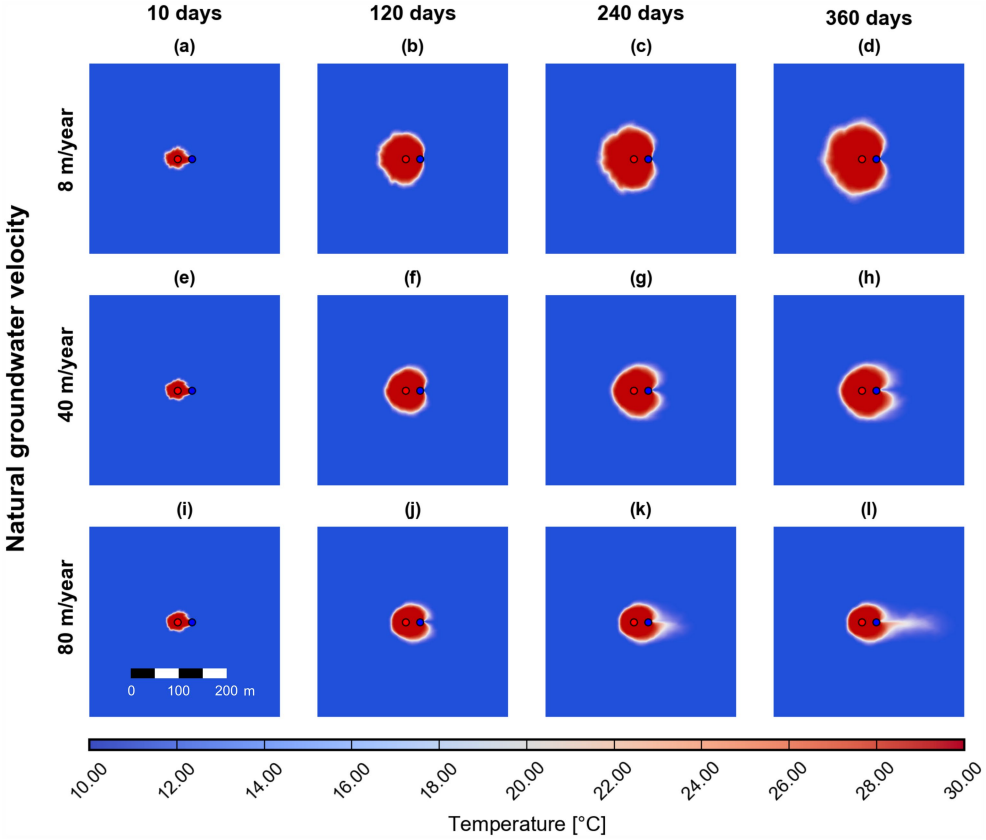

FIGURE 5
Simulated field-scale surface maps of temperature at three different natural groundwater flow velocities (scenarios S0 **(a–d)**, S1a **(e–h)**, and S1b **(i–l)**) at 10, 120, 240, and 360 days. The pumping rate is constant at 15 m^3/hour. Red and blue dots indicate the injection and extraction wells, respectively.

The reactive transport of the chlorinated ethenes was simulated in the solute transport domain, including the sequential dehalogenation of TCE to ethene and the non-isothermal kinetics observed in the microcosm experiments. Figure 7 shows the simulated surface maps of chlorinated ethene concentrations after 360 days at the four simulated injection temperatures (10°C, 20°C, 30°C, and 40°C). In Figure 7, the injection of groundwater with a temperature of 10°C can be considered the isothermal case, since the pristine groundwater temperature in the entire model domain is also 10°C. The degradation efficiency at 10°C is very low; only small amounts of TCE are transformed to cis-DCE and VC, with no ethene formed in the domain after 360 days (Figures 7a–d). The dehalogenation process is incomplete because the maximum specific degradation rate is low at a groundwater temperature of 10°C.

On the contrary, the injection of 20°C and 30°C warm groundwater into the contaminated aquifer results in non-isothermal transport phenomena leading to enhanced biotransformation and almost complete dechlorination from TCE to ethene (Figures 7e–l). The produced ethene might undergo transport and mass transfer processes (e.g., from the water to the gaseous phase, particularly in the shallow portion of the aquifer close to the unsaturated zone), but it could also be further biotransformed by indigenous microorganisms present in the aquifer. These visual results are supported by the evaluation of the total masses of the chlorinated ethenes in the domain, where the scenarios at 20°C and 30°C show the best bioremediation efficiency. The injection of groundwater with a temperature of 40°C results in a more efficient dehalogenation compared to the scenario at 10°C, but the transformation from TCE to ethene is incomplete. Note that contrary to the batch experiments, where no biotransformation of TCE was observed at 40°C, the injection of warm groundwater at 40°C into the multi-dimensional domain leads to zones of optimal thermal conditions for microbial growth and contaminant dehalogenation at the fringes of the heat plume. Over the simulated time, the heat plume spreads into the aquifer. The highly bioreactive zones at the fringes of the heat plume expand, finally resulting in the spatial distribution of contaminants as shown in Figures 7m–p. In contrast, the biological dehalogenation at 10°C (scenario S3a) is a scenario considering isothermal conditions, resulting in uniform, low degradation rates across the entire domain. The complex interplay between heat transport and microbial dehalogenation governs the mobility and fate of the contaminants in the multi-dimensional aquifer systems considered in this study.

3.2.3 Effect of scenario parameters on contaminant mass

The total masses of the chlorinated ethenes were evaluated in the entire solute transport domain, allowing a quantitative interpretation of the efficiency of bioremediation for the different scenarios listed in Table 1. First, the effect of the natural groundwater flow velocity on the overall bioremediation efficiency is analyzed. The flow velocity

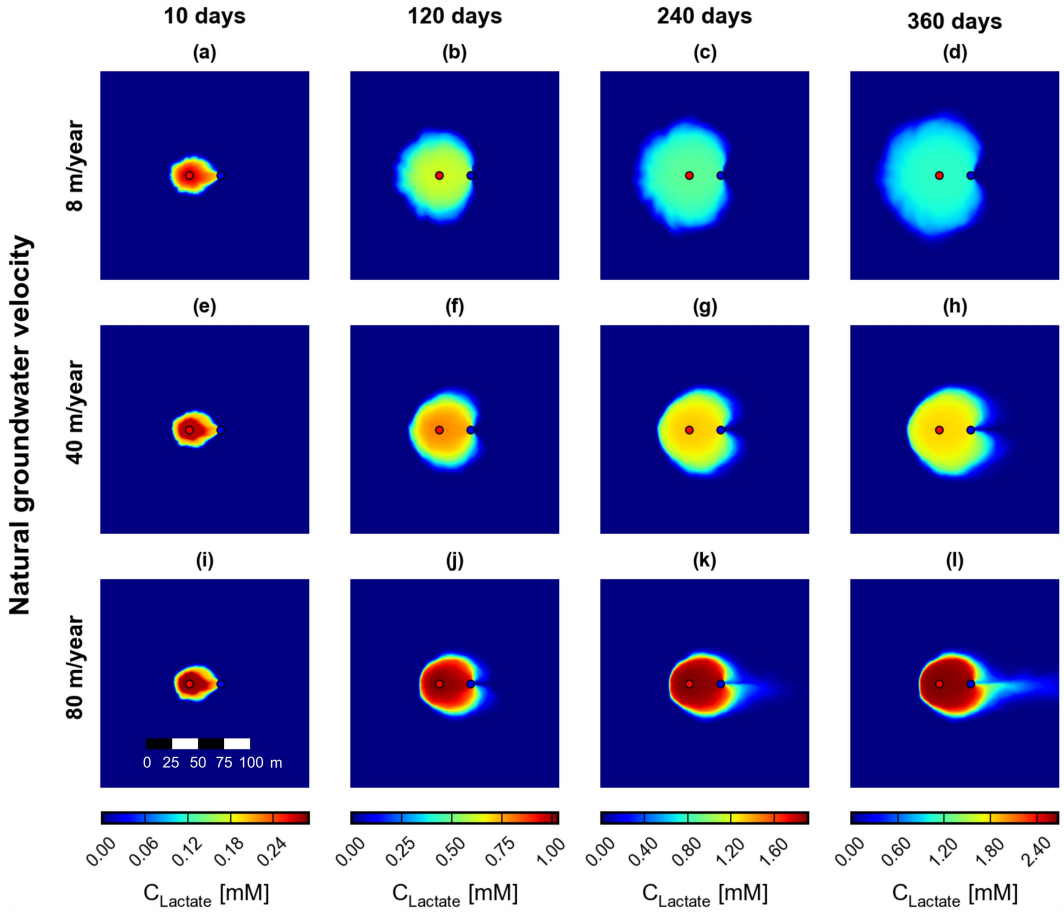

FIGURE 6
Simulated field-scale surface maps of lactate at three different natural groundwater flow velocities (scenarios S0 **(a–d)**, S1a **(e–h)**, and S1b **(i–l)**) at 10, 120, 240, and 360 days. Red and blue dots indicate the injection and extraction wells, respectively.

influences the total dehalogenation efficiency of cis-DCE and VC, with less pronounced effects for ethene (Figure 8). This faster biotransformation might be caused by increased mixing at higher groundwater flow velocities (Rolle and Kitanidis, 2014). In the Supplementary material we provide more information on the effect of the natural groundwater flow velocity on the efficiency of the ATES-ISB system (Supplementary Figure S4).

Secondly, we investigated the effect of the pumping rate of the injection/extraction system on the overall biotransformation efficiency. Figure 9 illustrates that a high pumping rate of 15 m^3/h is preferable at the beginning of the ATES-ISB intervention. However, after 150 to 200 days, the efficiency of scenarios considering lower pumping rates is comparable to scenarios with a higher pumping rate for most of the chlorinated ethenes investigated in this study. The pumping rate is strongly coupled to the natural groundwater flow velocity as shown in Figure 4. Furthermore, in this work, the pumping rate highly affects the amount of lactate injected into the aquifer system, which might explain the more efficient mass destruction of chlorinated ethenes at higher pumping rates because in fact more lactate is delivered into the contaminated aquifer (e.g., Figure 9a).

Thirdly, the temperature of the injected groundwater was varied, and the total contaminant masses were evaluated. Figure 10 shows the results of different injection temperatures and is linked to Figure 7, which shows surface maps of the identical scenarios. The isothermal scenario at 10°C shows slow biotransformation kinetics with incomplete transformation of TCE to ethene. In contrast, almost complete dehalogenation to the non-toxic end product ethene is observed considering an injection temperature of 20°C and 30°C. However, both scenarios show that VC is not completely transformed to ethene. The injection of 40°C warm groundwater leads to an improved mass destruction of TCE compared to the isothermal scenario (10°C), but to an accumulation of cis-DCE and VC up to 150 days, and 200 days, respectively (Figures 10b,c). This phenomenon is caused by the successive spreading of the injected 40°C heat plume into the aquifer, which results in bioreactive zones at the fringes of the expanding heat plume, where optimal conditions for microbial reductive dehalogenation are present. This dynamic system results, however, in incomplete biotransformation of TCE to ethene. Vinyl chloride concentrations in scenario S3c show, for example, the highest concentrations among all scenarios assessed in Figure 10 at the end of the simulation after 360 days (red solid line in Figure 10). In conclusion, the results show that the injected groundwater temperature strongly affects the dehalogenation efficiency in the considered ATES-ISB system.

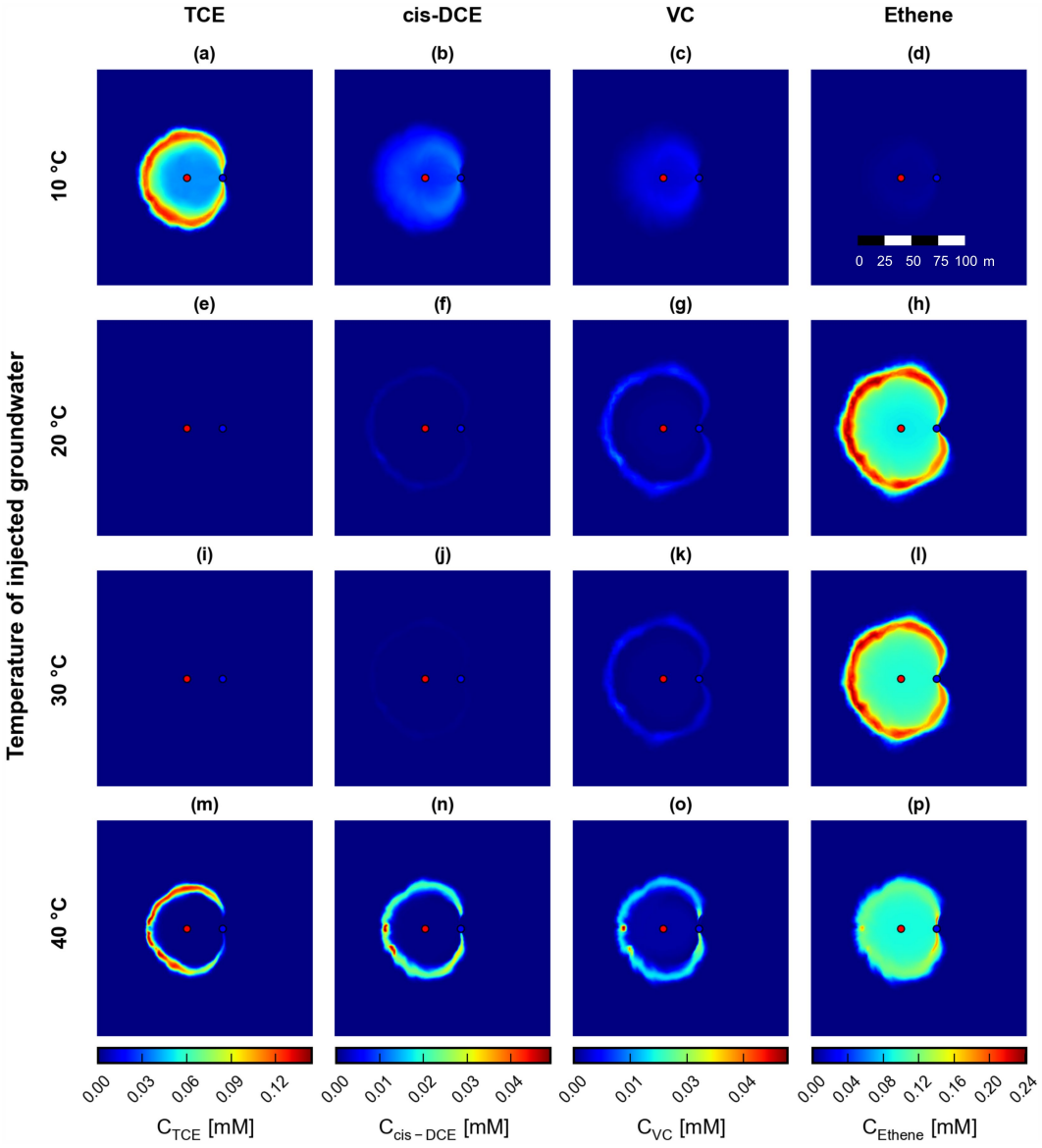

FIGURE 7
Simulated surface maps of chlorinated ethene concentrations at four different groundwater injection temperatures (rows) (scenarios S3a **(a–d)**, S3b **(e–h)**, S0 **(i–l)**, and S3c **(m–p)**) at the end of the simulations at 360 days. Red and blue dots indicate the injection and extraction wells, respectively.

Lastly, the impact of different lactate concentrations on the bioremediation efficiency of ATES-ISB interventions was investigated. Figure 11 shows the total masses of chlorinated ethenes over time considering three concentrations (0.002 mM, 0.02 mM, and 0.2 mM) of lactate injected into the simulated, polluted aquifer. Higher lactate concentrations are associated with faster and more complete contaminant mass destruction for all contaminants (TCE, cis-DCE, VC), and more efficient production of non-toxic ethene. The apparent effect of the added electron donor source suggests that lactate is limiting the extent of microbial reductive dechlorination in the ATES-ISB system considered in this study. The efficient delivery of lactate (or other suitable carbon sources) in the contaminated aquifer seems to be particularly important for the overall bioremediation efficiency of the simulated remediation system.

4 Conclusions

In this study, we presented a process-based modeling framework for the interpretation and analysis of temperature-dependent biotransformation of chlorinated ethenes. The proposed model is capable of simulating biodegradation in batch microcosms, as well as field-scale reactive transport of Aquifer Thermal Energy Storage combined with *in situ* bioremediation (ATES-ISB), which is a promising remediation technique to foster more sustainable and efficient groundwater clean-up. The modeling framework described

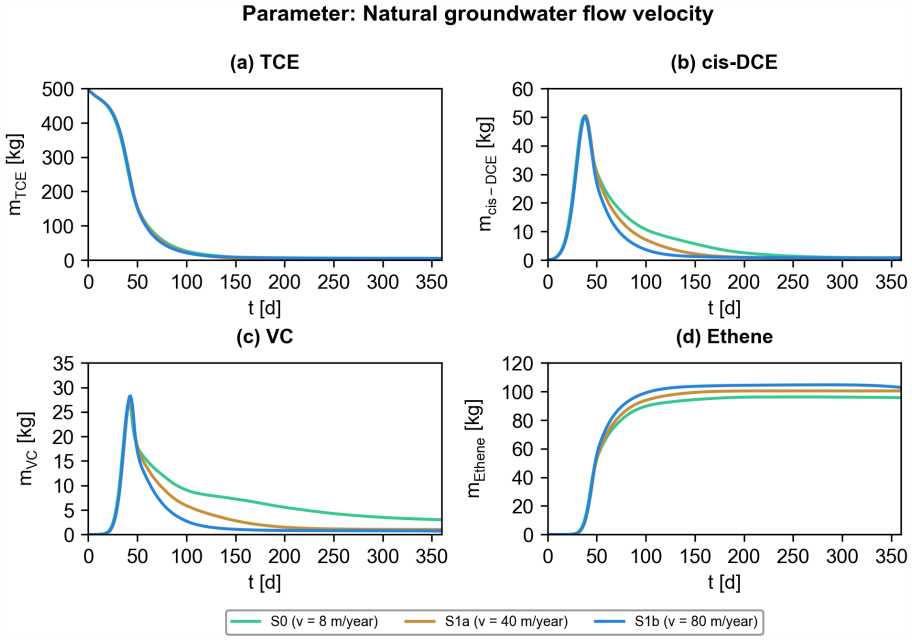

FIGURE 8
Effect of different natural groundwater flow velocities on bioremediation efficiency. Simulated contaminant mass of chlorinated ethenes ((**a**) TCE; (**b**) cis-DCE; (**c**) VC; (**d**) ethene) for scenarios S0, S1a, and S1b.

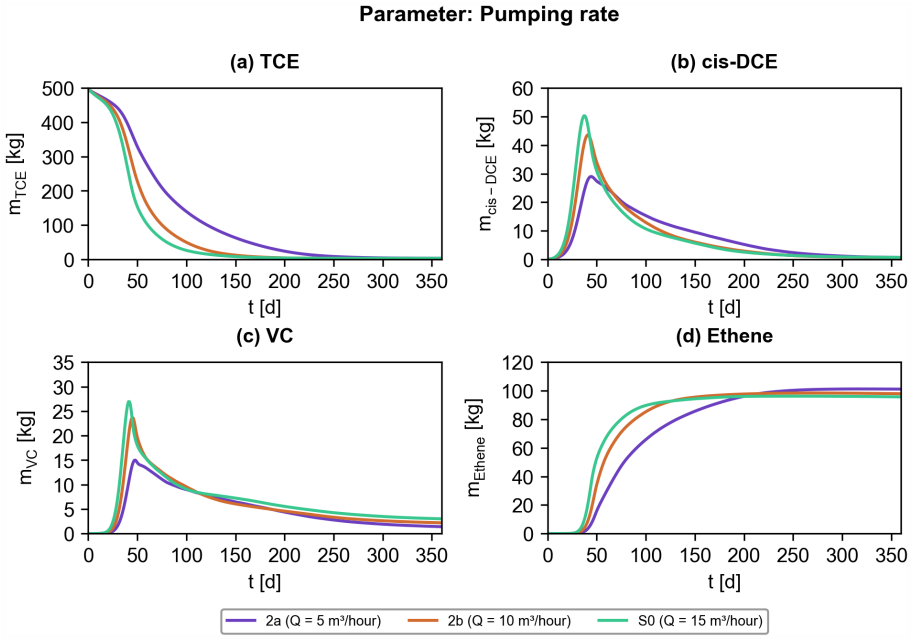

FIGURE 9
Effect of different pumping rates on bioremediation efficiency. Simulated contaminant mass of chlorinated ethenes ((**a**) TCE; (**b**) cis-DCE; (**c**) VC; (**d**) ethene) for scenarios S2a, S2b, and S0.

in this study accounts for: (i) multi-phase mass transfer limitations and temperature-dependent microbial reductive dehalogenation in batch systems, and (ii) multi-dimensional non-isothermal fluid flow, heat transport, and reactive solute transport in physically and chemically heterogeneous groundwater systems in combination with temperature-dependent microbial growth kinetics and contaminant dehalogenation.

Experimental microcosm studies of temperature-dependent microbial reductive dechlorination of chlorinated ethenes were interpreted using the modeling approach proposed in this work. Maximum specific transformation rates were derived, which served as input for scenario simulations of an ATES-ISB system in a sandy heterogeneous aquifer contaminated with TCE. The scenario simulations, considering one site parameter (the natural

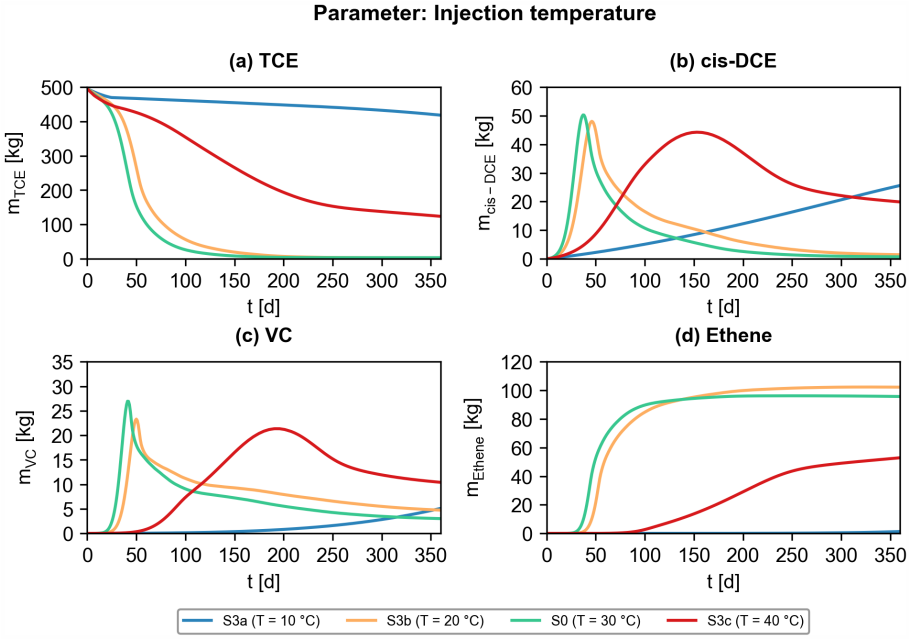

FIGURE 10
Effect of different injection temperatures on bioremediation efficiency. Simulated contaminant mass of chlorinated ethenes (**(a)** TCE; **(b)** cis-DCE; **(c)** VC; **(d)** ethene) for scenarios S3a, S3b, S0 and S3c (also depicted in Figure 7).

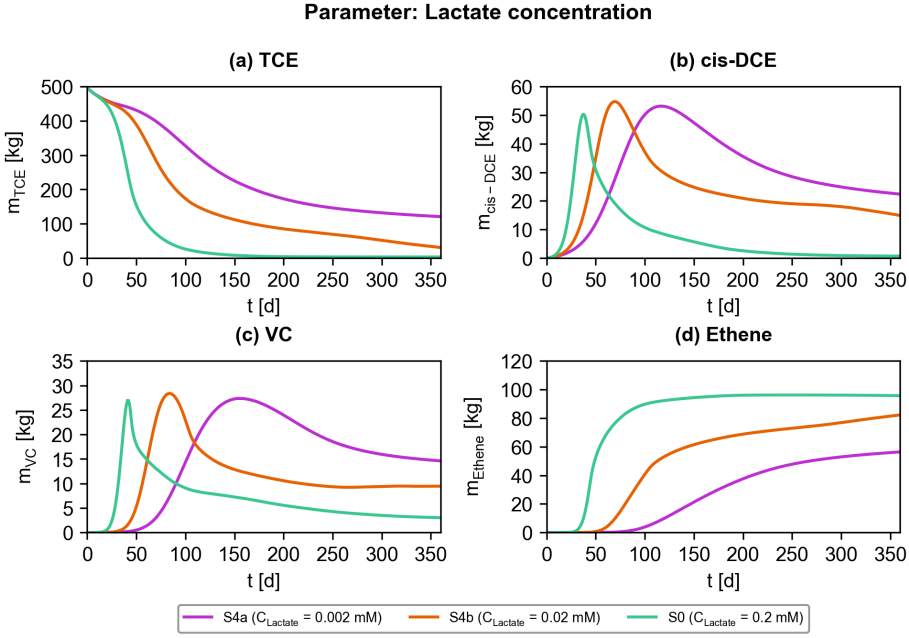

FIGURE 11
Effect of different injected lactate concentrations on bioremediation efficiency. Simulated contaminant mass of chlorinated ethenes (**(a)** TCE; **(b)** cis-DCE; **(c)** VC; **(d)** ethene) for scenarios S4a, S4b, and S0.

groundwater flow velocity) and three operational parameters (the pumping rate of the injection/extraction system, the temperature of injected groundwater, and the concentration of the injected lactate) were carried out to identify optimal conditions for efficient ATES-ISB interventions in polluted subsurface porous media. The scenario simulations highlight the importance of the injection temperature and the concentration of the injected lactate for complete dehalogenation of chlorinated ethenes in the considered heterogeneous aquifer system. The natural groundwater flow velocity, i.e., the groundwater velocity without active pumping, as well as the pumping rate of the ATES-ISB system were found to be of lower significance for efficient

remediation of the aquifer considered in this study. The natural groundwater flow velocity and pumping rate are, nonetheless, important since they control the delivery of the injected heated water and solutes in the aquifer. Future investigation should address more explicitly the interplay between non-isothermal biodegradation and groundwater chemistry to explore the interactions between the beneficial effects of ATES-related higher temperatures for *in situ* chlorinated compounds biotransformation with concurrent effects of increased temperature in shallow aquifers. The latter include the potential release of dissolved organic carbon (Brons et al., 1991; Jesußek et al., 2013), which could provide electron donor and substrate to sustain reductive dehalogenation, as well as of metals and metalloids that could impact bacteria activity and groundwater quality (Bonte et al., 2013; Lüders et al., 2020).

This scenario modeling study explored the feasibility of ATES-ISB approaches by combining non-isothermal microcosm reductive dehalogenation and field-scale reactive transport modeling. The interplay of temperature-dependent physical, chemical, and biological processes controls the bioremediation efficiency of such ATES-ISB interventions. The modeling framework described in this work is helpful for the identification of controlling mechanisms and optimal parameters in complex subsurface remediation systems, such as ATES-ISB. Furthermore, the developed modeling approach can be used for planning, designing, and guiding remediation setups for non-isothermal bioremediation interventions.

Data availability statement

The original contributions presented in the study are included in the article/Supplementary material, further inquiries can be directed to the corresponding author.

Author contributions

HW: Conceptualization, Data curation, Formal analysis, Investigation, Methodology, Software, Validation, Visualization, Writing – original draft. MB: Conceptualization, Data curation, Investigation, Writing – review & editing. KM: Conceptualization, Methodology, Supervision, Writing – review & editing. CV: Conceptualization, Writing – review & editing. IN: Conceptualization, Resources, Writing – review & editing. MR: Conceptualization, Funding acquisition, Methodology, Resources, Supervision, Writing – review & editing.

Funding

The author(s) declare that financial support was received for the research, authorship, and/or publication of this article. This work was supported by the Independent Research Fund Denmark (project BiodegrATES, grant DFF 0136-00205B).

Conflict of interest

The authors declare that the research was conducted in the absence of any commercial or financial relationships that could be construed as a potential conflict of interest.

The reviewer ZN is currently organizing a Research Topic with the author IN.

Publisher's note

Supplementary material

The Supplementary material for this article can be found online at: https://www.frontiersin.org/articles/10.3389/frwa.2025.1499448/full#supplementary-material

References

Aeppli, C., Berg, M., Cirpka, O. A., Holliger, C., Schwarzenbach, R. P., and Hofstetter, T. B. (2009). Influence of mass-transfer limitations on carbon isotope fractionation during microbial dechlorination of trichloroethene. *Environ. Sci. Technol.* 43, 8813–8820. doi: 10.1021/es901481b

Allen-King, R. M., Butler, B. J., and Reichert, B. (1995). Fate of the herbicide glufosinate-ammonium in the sandy, low-organic-carbon aquifer at CFB Borden, Ontario, Canada. *J. Contam. Hydrol.* 18, 161–179. doi: 10.1016/0169-7722(94)00046-K

Bauer, R. D., Rolle, M., Bauer, S., Eberhardt, C., Grathwohl, P., Kolditz, O., et al. (2009). Enhanced biodegradation by hydraulic heterogeneities in petroleum hydrocarbon plumes. *J. Contam. Hydrol.* 105, 56–68. doi: 10.1016/j.jconhyd.2008.11.004

Bear, J., and Bachmat, Y. (1990). Introduction to modeling of transport phenomena in porous media. Dordrecht: Springer Netherlands.

Beyer, C., Popp, S., and Bauer, S. (2016). Simulation of temperature effects on groundwater flow, contaminant dissolution, transport and biodegradation due to shallow geothermal use. *Environ. Earth Sci.* 75:1244. doi: 10.1007/s12665-016-5976-8

Bin Hudari, M. S., Deb, S., Vogt, C., Filippini, M., and Nijenhuis, I. (2025). "Temperature-associated effects on methanogenesis and microbial reductive dechlorination of trichloroethene in contaminated aquifer sediments" in Ed. Giuseppe O. *Frontiers in Water* in preparation for this Special Issue.

Bonte, M., van Breukelen, B. M., and Stuyfzand, P. J. (2013). Temperature-induced impacts on groundwater quality and arsenic mobility in anoxic aquifer sediments used for both drinking water and shallow geothermal energy production. *Water Res.* 47, 5088–5100. doi: 10.1016/j.watres.2013.05.049

Brons, H. J., Griffioen, J., Appelo, C. A. J., and Zehnder, A. J. B. (1991). (bio) geochemical reactions in aquifer material from a thermal energy storage site. *Water Res.* 25, 729–736. doi: 10.1016/0043-1354(91)90048-U

Chiogna, G., Eberhardt, C., Grathwohl, P., Cirpka, O. A., and Rolle, M. (2010). Evidence of compound-dependent hydrodynamic and mechanical transverse dispersion by multitracer laboratory experiments. *Environ. Sci. Technol.* 44, 688–693. doi: 10.1021/es9023964

Cupples, A. M., Spormann, A. M., and McCarty, P. L. (2004). Comparative evaluation of Chloroethene Dechlorination to Ethene by Dehalococcoides-like microorganisms. *Environ. Sci. Technol.* 38, 4768–4774. doi: 10.1021/es049965z

Epting, J., Händel, F., and Huggenberger, P. (2013). Thermal management of an unconsolidated shallow urban groundwater body. *Hydrol. Earth Syst. Sci.* 17, 1851–1869. doi: 10.5194/hess-17-1851-2013

Fletcher, K. E., Costanza, J., Pennell, K. D., and Löffler, F. E. (2011). Electron donor availability for microbial reductive processes following thermal treatment. *Water Res.* 45, 6625–6636. doi: 10.1016/j.watres.2011.09.033

Friis, A. K., Albrechtsen, H.-J., Heron, G., and Bjerg, P. L. (2005). Redox processes and release of organic matter after thermal treatment of a TCE-contaminated aquifer. *Environ. Sci. Technol.* 39, 5787–5795. doi: 10.1021/es048322g

Friis, A. K., Edwards, E. A., Albrechtsen, H. J., Udell, K. S., Duhamel, M., and Bjerg, P. L. (2007a). Dechlorination after thermal treatment of a TCE-contaminated aquifer: laboratory experiments. *Chemosphere* 67, 816–825. doi: 10.1016/j.chemosphere.2006.10.012

Friis, A. K., Heimann, A. C., Jakobsen, R., Albrechtsen, H. J., Cox, E., and Bjerg, P. L. (2007b). Temperature dependence of anaerobic TCE-dechlorination in a highly enriched Dehalococcoides-containing culture. *Water Res.* 41, 355–364. doi: 10.1016/j.watres.2006.09.026

Friis, A. K., Kofoed, J. L. L., Heron, G., Albrechtsen, H. J., and Bjerg, P. L. (2007c). Microcosm evaluation of bioaugmentation after field-scale thermal treatment of a TCE-contaminated aquifer. *Biodegradation* 18, 661–674. doi: 10.1007/s10532-006-9098-y

Griebler, C., and Lueders, T. (2009). Microbial biodiversity in groundwater ecosystems. *Freshw. Biol.* 54, 649–677. doi: 10.1111/j.1365-2427.2008.02013.x

Guedes de Carvalho, J. R. F., and Delgado, J. M. P. Q. (2005). Overall map and correlation of dispersion data for flow through granular packed beds. *Chem. Eng. Sci.* 60, 365–375. doi: 10.1016/j.ces.2004.07.121

Heldt, S., Beyer, C., and Bauer, S. (2024). Uncertainty assessment of thermal recovery and subsurface temperature changes induced by high-temperature aquifer thermal energy storage (HT-ATES): A case study. *Geothermics* 122:103086. doi: 10.1016/j.geothermics.2024.103086

Hood, E. D., Major, D. W., Quinn, J. W., Yoon, W.-S., Gavaskar, A., and Edwards, E. A. (2008). Demonstration of enhanced bioremediation in a TCE source area at launch complex 34, Cape Canaveral air Force Station. *Groundwater Monit. Remediat.* 28, 98–107. doi: 10.1111/j.1745-6592.2008.00197.x

Hunkeler, D., Aravena, R., and Butler, B. J. (1999). Monitoring microbial dechlorination of tetrachloroethene (PCE) in groundwater using compound-specific stable carbon isotope ratios: microcosm and field studies. *Environ. Sci. Technol.* 33, 2733–2738. doi: 10.1021/es981282u

IAPWS (2007). Revised release R7-97 on the IAPWS industrial formulation 1997 for the thermodynamic properties of water and steam. Lucerne, Switzerland: International Association for the Properties of Water and Steam.

Illy, V. D., Cohen, G. J. V., Verardo, E., Höhener, P., Guiserix, N., and Atteia, O. (2022). Using 1,1,1-Trichloroethane degradation data to understand NAPL dissolution and solute transport at real sites. *J. Contam. Hydrol.* 245:103934. doi: 10.1016/j.jconhyd.2021.103934

Jesußek, A., Grandel, S., and Dahmke, A. (2013). Impacts of subsurface heat storage on aquifer hydrogeochemistry. *Environ. Earth Sci.* 69, 1999–2012. doi: 10.1007/s12665-012-2037-9

Jin, B., Haderlein, S. B., and Rolle, M. (2013). Integrated carbon and chlorine isotope modeling: applications to chlorinated aliphatic hydrocarbons dechlorination. *Environ. Sci. Technol.* 47, 1443–1451. doi: 10.1021/es304053h

Jin, B., Rolle, M., Li, T., and Haderlein, S. B. (2014). Diffusive fractionation of BTEX and chlorinated ethenes in aqueous solution: quantification of spatial isotope gradients. *Environ. Sci. Technol.* 48, 6141–6150. doi: 10.1021/es4046956

Koproch, N., Dahmke, A., and Köber, R. (2019). The aqueous solubility of common organic groundwater contaminants as a function of temperature between 5 and 70 °C. *Chemosphere* 217, 166–175. doi: 10.1016/j.chemosphere.2018.10.153

Kumar, R., Sonnenthal, E. L., Smith, J. T., Nico, P. S., and Dobson, P. F. (2024). Reactive transport modeling of the aquifer thermal energy storage (ATES) system at Stockton university New Jersey during seasonal operations. *Geothermics* 123:103121. doi: 10.1016/j.geothermics.2024.103121

Lüders, K., Dahmke, A., Fiedler, M., and Köber, R. (2020). Temperature influence on mobilisation and (re)fixation of trace elements and heavy metals in column tests with aquifer sediments from 10 to 70 °C. *Water Res.* 169:115266. doi: 10.1016/j.watres.2019.115266

Major, D. W., McMaster, M. L., Cox, E. E., Edwards, E. A., Dworatzek, S. M., Hendrickson, E. R., et al. (2002). Field demonstration of successful bioaugmentation to achieve Dechlorination of Tetrachloroethene to Ethene. *Environ. Sci. Technol.* 36, 5106–5116. doi: 10.1021/es0255711

Malaguerra, F., Chambon, J. C., Bjerg, P. L., Scheutz, C., and Binning, P. J. (2011). Development and sensitivity analysis of a fully kinetic model of sequential reductive dechlorination in groundwater. *Environ. Sci. Technol.* 45, 8395–8402. doi: 10.1021/es201270z

Marcet, T. F., Cápiro, N. L., Yang, Y., Löffler, F. E., and Pennell, K. D. (2018). Impacts of low-temperature thermal treatment on microbial detoxification of tetrachloroethene under continuous flow conditions. *Water Res.* 145, 21–29. doi: 10.1016/j.watres.2018.07.076

McCarty, P. L. (2010). "Groundwater contamination by chlorinated solvents: history, remediation technologies and strategies" in In situ remediation of chlorinated solvent plumes. eds. H. F. Stroo and C. H. Ward (New York, NY: Springer), 1–28.

Meng, B., Yang, Y., Huang, Y., Kolditz, O., and Shao, H. (2021). Remediation potential of borehole thermal energy storage for chlorinated hydrocarbon plumes: numerical modeling in a variably-saturated aquifer. *Front. Earth Sci.* 9, 1–17. doi: 10.3389/feart.2021.790315

Molz, F. J., Parr, A. D., and Andersen, P. F. (1981). Thermal energy storage in a confined aquifer: second cycle. *Water Resour. Res.* 17, 641–645. doi: 10.1029/WR017i003p00641

Muniruzzaman, M., and Rolle, M. (2017). Experimental investigation of the impact of compound-specific dispersion and electrostatic interactions on transient transport and solute breakthrough. *Water Resour. Res.* 53, 1189–1209. doi: 10.1002/2016WR019727

Murray, A. M., Maillard, J., Jin, B., Broholm, M. M., Holliger, C., and Rolle, M. (2019). A modeling approach integrating microbial activity, mass transfer, and geochemical processes to interpret biological assays: an example for PCE degradation in a multi-phase batch setup. *Water Res.* 160, 484–496. doi: 10.1016/j.watres.2019.05.087

Murray, A., Maillard, J., Rolle, M., Broholm, M., and Holliger, C. (2020). Impact of iron- and/or sulfate-reduction on a cis-1,2-dichloroethene and vinyl chloride respiring bacterial consortium: experiments and model-based interpretation. *Environ. Sci.* 22, 740–750. doi: 10.1039/c9em00544g

Němeček, J., Steinová, J., Špánek, R., Pluhař, T., Pokorný, P., Najmanová, P., et al. (2018). Thermally enhanced in situ bioremediation of groundwater contaminated with chlorinated solvents – A field test. *Sci. Total Environ.* 622-623, 743–755. doi: 10.1016/j.scitotenv.2017.12.047

Ni, Z., van Gaans, P., Rijnaarts, H., and Grotenhuis, T. (2018). Combination of aquifer thermal energy storage and enhanced bioremediation: biological and chemical clogging. *Sci. Total Environ.* 614, 707–713. doi: 10.1016/j.scitotenv.2017.09.087

Ni, Z., Van Gaans, P., Smit, M., Rijnaarts, H., and Grotenhuis, T. (2015). Biodegradation of *cis* −1,2-Dichloroethene in simulated underground thermal energy storage systems. *Environ. Sci. Technol.* 49, 13519–13527. doi: 10.1021/acs.est.5b03068

Nijenhuis, I., Nikolausz, M., Köth, A., Felföldi, T., Weiss, H., Drangmeister, J., et al. (2007). Assessment of the natural attenuation of chlorinated ethenes in an anaerobic contaminated aquifer in the Bitterfeld/Wolfen area using stable isotope techniques, microcosm studies and molecular biomarkers. *Chemosphere* 67, 300–311. doi: 10.1016/j.chemosphere.2006.09.084

Nijenhuis, I., Schmidt, M., Pellegatti, E., Paramatti, E., Richnow, H. H., and Gargini, A. (2013). A stable isotope approach for source apportionment of chlorinated ethene plumes at a complex multi-contamination events urban site. *J. Contam. Hydrol.* 153, 92–105. doi: 10.1016/j.jconhyd.2013.06.004

Ottosen, C. B., Bjerg, P. L., Hunkeler, D., Zimmermann, J., Tuxen, N., Harrekilde, D., et al. (2021). Assessment of chlorinated ethenes degradation after field scale injection of activated carbon and bioamendments: application of isotopic and microbial analyses. *J. Contam. Hydrol.* 240:103794. doi: 10.1016/j.jconhyd.2021.103794

Pankow, J. F., and Cherry, J. A. (1996). Dense chlorinated solvents and other DNAPLs in groundwater. Portland, OR: Waterloo Press.

Popp, S., Beyer, C., Dahmke, A., and Bauer, S. (2015). Model development and numerical simulation of a seasonal heat storage in a contaminated shallow aquifer. *Energy Procedia* 76, 361–370. doi: 10.1016/j.egypro.2015.07.842

Powers, S. E., Abriola, L. M., Dunkin, J. S., and Weber, W. J. (1994). Phenomenological models for transient NAPL-water mass-transfer processes. *J. Contam. Hydrol.* 16, 1–33. doi: 10.1016/0169-7722(94)90070-1

Rolle, M., Chiogna, G., Hochstetler, D. L., and Kitanidis, P. K. (2013). On the importance of diffusion and compound-specific mixing for groundwater transport: an investigation from pore to field scale. *J. Contam. Hydrol.* 153, 51–68. doi: 10.1016/j.jconhyd.2013.07.006

Rolle, M., Hochstetler, D., Chiogna, G., Kitanidis, P. K., and Grathwohl, P. (2012). Experimental investigation and pore-scale modeling interpretation of compound-specific transverse dispersion in porous media. *Transp. Porous Media* 93, 347–362. doi: 10.1007/s11242-012-9953-8

Rolle, M., and Kitanidis, P. K. (2014). Effects of compound-specific dilution on transient transport and solute breakthrough: A pore-scale analysis. *Adv. Water Resour.* 71, 186–199. doi: 10.1016/j.advwatres.2014.06.012

Rolle, M., and Le Borgne, T. (2019). Mixing and reactive fronts in the subsurface. *Rev. Mineral. Geochem.* 85, 111–142. doi: 10.2138/rmg.2018.85.5

Roohidehkordi, I., and Krol, M. M. (2021). Applicability of ground source heat pumps as a bioremediation-enhancing technology for monoaromatic hydrocarbon contaminants. *Sci. Total Environ.* 778:146235. doi: 10.1016/j.scitotenv.2021.146235

Rosenberg, L., Mosthaf, K., Broholm, M. M., Fjordbøge, A. S., Tuxen, N., Kerrn-Jespersen, I. H., et al. (2023). A novel concept for estimating the contaminant mass discharge of chlorinated ethenes emanating from clay till sites. *J. Contam. Hydrol.* 252:104121. doi: 10.1016/j.jconhyd.2022.104121

Rosso, L., Lobry, J. R., Bajard, S., and Flandrois, J. P. (1995). Convenient model to describe the combined effects of temperature and pH on microbial growth. *Appl. Environ. Microbiol.* 61, 610–616. doi: 10.1128/aem.61.2.610-616.1995

Scheutz, C., Durant, N. D., and Broholm, M. M. (2014). Effects of bioaugmentation on enhanced reductive dechlorination of 1,1,1-trichloroethane in groundwater: a comparison of three sites. *Biodegradation* 25, 459–478. doi: 10.1007/s10532-013-9674-x

Scheutz, C., Durant, N. D., Dennis, P., Hansen, M. H., Jørgensen, T., Jakobsen, R., et al. (2008). Concurrent Ethene generation and growth of Dehalococcoides containing vinyl

chloride reductive dehalogenase genes during an enhanced reductive Dechlorination field demonstration. *Environ. Sci. Technol.* 42, 9302–9309. doi: 10.1021/es800764t

Sprocati, R., Gallo, A., Wienkenjohann, H., and Rolle, M. (2023). Temperature-dependent dynamics of electrokinetic conservative and reactive transport in porous media: A model-based analysis. *J. Contam. Hydrol.* 259:104261. doi: 10.1016/j.jconhyd.2023.104261

Stroo, H. F., Major, D. W., and Gossett, J. M. (2010). "Bioaugmentation for anaerobic bioremediation of chlorinated solvents" in In situ remediation of chlorinated solvent plumes. eds. H. F. Stroo and C. H. Ward (New York, NY: Springer), 425–454.

Sudicky, E. A. (1986). A natural gradient experiment on solute transport in a sand aquifer: spatial variability of hydraulic conductivity and its role in the dispersion process. *Water Resour. Res.* 22, 2069–2082. doi: 10.1029/WR022i013p02069

Ueckert, M., and Baumann, T. (2019). Hydrochemical aspects of high-temperature aquifer storage in carbonaceous aquifers: evaluation of a field study. *Geotherm. Energy* 7, 1–22. doi: 10.1186/s40517-019-0120-0

Valocchi, A. J., Bolster, D., and Werth, C. J. (2019). Mixing-limited reactions in porous media. *Transp. Porous Media* 130, 157–182. doi: 10.1007/s11242-018-1204-1

Wagner, W., Cooper, J. R., Dittmann, A., Kijima, J., Kretzschmar, H.-J., Kruse, A., et al. (2000). The IAPWS industrial formulation 1997 for the thermodynamic properties of water and steam. *J. Eng. Gas Turbines Power* 122, 150–184. doi: 10.1115/1.483186

Wienkenjohann, H., Jin, B., and Rolle, M. (2023). Diffusive-dispersive isotope fractionation of chlorinated Ethenes in groundwater: the key role of incomplete mixing and its multi-scale effects. *Water Resour. Res.* 59:e2022WR034041. doi: 10.1029/2022WR034041

Wienkenjohann, H., Mosthaf, K., Fischer, L. M., Bennedsen, L., Flyvbjerg, J., Christophersen, M., et al. (2024). Low-temperature aquifer thermal energy storage combined with in situ bioremediation of chlorinated ethenes: pilot-scale observations and model-based interpretation. *J. Contam. Hydrol.* 267:104421. doi: 10.1016/j.jconhyd.2024.104421

Worch, E. (1993). Eine neue Gleichung zur Berechnung von Diffusionskoeffizienten gelöster Stoffe. *Vom Wasser* 81, 289–297.

Yamazaki, Y., Hasegawa, A., Tian, X., Suzuki, I., Kobayashi, T., Shimizu, T., et al. (2020). Effect of elevated temperature on cis-1,2-dichloroethene dechlorination and microbial community structure in contaminated soils—A biostimulation approach. *J. Environ. Chem. Eng.* 8:103682. doi: 10.1016/j.jece.2020.103682

Ye, Y., Chiogna, G., Cirpka, O. A., Grathwohl, P., and Rolle, M. (2015). Experimental investigation of compound-specific dilution of solute plumes in saturated porous media: 2-D vs. 3-D flow-through systems. *J. Contam. Hydrol.* 172, 33–47. doi: 10.1016/j.jconhyd.2014.11.002

Yu, R., Andrachek, R. G., Lehmicke, L. G., and Freedman, D. L. (2018). Remediation of chlorinated ethenes in fractured sandstone by natural and enhanced biotic and abiotic processes: A crushed rock microcosm study. *Sci. Total Environ.* 626, 497–506. doi: 10.1016/j.scitotenv.2018.01.064

Yu, S., and Semprini, L. (2004). Kinetics and modeling of reductive dechlorination at high PCE and TCE concentrations. *Biotechnol. Bioeng.* 88, 451–464. doi: 10.1002/bit.20260

Zeman, N. R., Irianni Renno, M., Olson, M. R., Wilson, L. P., Sale, T. C., and De Long, S. K. (2014). Temperature impacts on anaerobic biotransformation of LNAPL and concurrent shifts in microbial community structure. *Biodegradation* 25, 569–585. doi: 10.1007/s10532-014-9682-5

Zimmerman, R. W. (1989). Thermal conductivity of fluid-saturated rocks. *J. Pet. Sci. Eng.* 3, 219–227. doi: 10.1016/0920-4105(89)90019-3

Zuurbier, K. G., Hartog, N., Valstar, J., Post, V. E. A., and van Breukelen, B. M. (2013). The impact of low-temperature seasonal aquifer thermal energy storage (SATES) systems on chlorinated solvent contaminated groundwater: modeling of spreading and degradation. *J. Contam. Hydrol.* 147, 1–13. doi: 10.1016/j.jconhyd.2013.01.002